A Review of Hybrid Topologies Combining Line-Commutated and Cascaded Full-Bridge Converters

Panagiotis Bakas, *Student Member, IEEE,* Lennart Harnefors, *Senior Member, IEEE,*
Staffan Norrga, *Member, IEEE,* Alireza Nami, *Senior Member, IEEE,* Kalle Ilves, *Member, IEEE,*
Frans Dijkhuizen, *Member, IEEE,* and Hans-Peter Nee, *Senior Member, IEEE*

Note that this version of the paper is not the same as the latest version, which can be found in IEEE Xplore.

***Abstract*—This paper presents a review of concepts for enabling the operation of a line-commutated converter (LCC) at leading power angles. These concepts rely on voltage or current injection at the ac or dc sides of the LCC, which can be achieved in different ways. We focus on the voltage and current injection by full-bridge (FB) arms, which can be connected either at the ac or dc sides of the LCC and can generate voltages that approximate ideal sinusoids. Hybrid configurations of an LCC connected at the ac side in series or in parallel with FB arms are presented. Moreover, a hybrid configuration of an LCC connected in parallel at the ac side and in series at the dc side with an FB modular multilevel converter (MMC) is outlined. The main contribution of this paper is an analysis and comparison of the mentioned hybrid configurations in terms of the capability to independently control the active (P) and reactive power (Q).**

***Index Terms*—DC-AC power converters, HVDC transmission, Static VAr compensators**

I. Introduction

THE thyristor-based line-commutated converter (LCC) has been employed since the 1960s for enabling the high-voltage dc (HVDC) transmission. LCCs are operating only at lagging power angles due to their dependence on the grid voltage for commutation. The reactive-power consumption is usually quite high and should be supplied by the grid or by capacitor banks. The problem has been addressed already [1], [2]. The main idea is the injection of a voltage pulse in series with the commutation voltage. This voltage pulse should be injected during the commutation interval, when the phase current is not zero. This implies that there is an energy transfer between the main circuit and the source injecting the voltage pulse. Thus, an active energy source is required.

An alternative idea devoid of an active energy source is the capacitor-commutated converter (CCC) [3]–[5]. The introduction of a series capacitor enables the CCC to operate at leading power angles, but the uncontrollable capacitor-injected voltages lead to commutation failure after a grid fault [6]. This can be avoided by the addition of a three-phase voltage-source converter (VSC), which is able to control the injected voltages, acting as an active capacitor [6]. This is termed an active-capacitor commutated converter (ACC).

Recently, the ideas of using a FB VSC as an active capacitor or as a source of voltage pulses have been proposed in [7] and [8] respectively. In [7] it is shown that the capacitance of the full-bridge can be significantly reduced by employing special modulation techniques, which account for variations of the capacitor voltage. In [8] the alternative concept of voltage-pulse injection is analyzed. This concept in this paper is similar to that in [1], [2], with the difference that the voltage-pulse injection is implemented by single-phase full-bridge (FB) VSCs and does not require an active energy source. This implementation requires less capacitance and is more compact than a CCC. However, the voltage rating of the FB VSC in both [7] and [8] needs to be relatively high, implying the need for series connection of semiconductor devices.

Shunt-current injection is another alternative [9]–[13] that uses a static var compensator (SVC) or a VSC connected at the ac side of an LCC. The concept is extended in [14]–[17] by connecting a two-level VSC in series at the dc side and in parallel at the ac side of the LCC. Compensation of either reactive power [15]–[17] or current harmonics [14] is achieved by injecting current at the ac side, while contributing to the active-power transfer via the series connection at the dc side.

In general, cascaded FB converters, termed FB arms, are capable of generating voltages that approximate ideal sinusoids and thus, can be used to inject sinusoidal voltages or currents with reduced filtering requirements, as shown in [20]. Therefore, in this paper, the series voltage injection and shunt current injection concepts for reactive-power compensation of the LCC are revised by replacing the VSCs with FB arms [21], [22]. More specifically, the three-phase VSC and the capacitors of the ACC, as well as the shunt-connected VSC are replaced by FB arms per phase. These hybrid topologies of FB arms and the FB MMC with an LCC are presented in this paper.

The main contribution of this paper is the comprehensive analysis and comparison of these hybrid topologies in terms of dimensioning and PQ capability, i.e., the extent to which active (P) and reactive (Q) power can be controlled independently. The analysis consists of: 1) the investigation of the operational characteristics; and 2) the derivation of the equations that

Manuscript sent June 3, 2016.

P. Bakas and L. Harnefors are with ABB Corporate Research, Västerås 721 78, Sweden and the Royal Institute of Technology (KTH), Stockholm 100 44, Sweden (e-mail: pbakas@kth.se; lennart.harnefors@se.abb.com).

S. Norrga and H.-P. Nee are with the Royal Institute of Technology (KTH), Stockholm 100 44, Sweden (e-mail: norrga@kth.se).

A. Nami, K. Ilves and F. Dijkhuizen are with ABB Corporate Research, Västerås 721 78, Sweden (e-mail: alireza.nami@se.abb.com, kalle.ilves@se.abb.com, frans.r.dijkhuizen@se.abb.com).

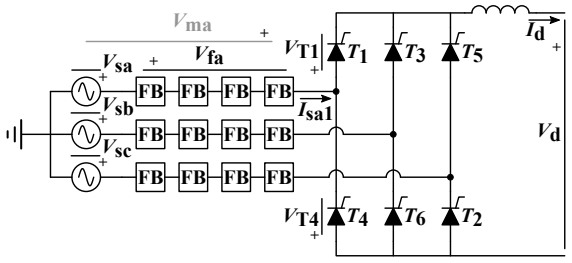

Fig. 1. SAC topology: LCC with FB arms connected in series at the ac side.

yield the voltage and current ratings of the FB arms for each hybrid topology. Moreover, the rating equations are used for analyzing and comparing the PQ capability of the mentioned hybrid topologies. To the best knowledge of the authors, such a comprehensive analysis and comparison has not been presented before.

The outline of this paper is as follows. In Section II the hybrid topologies are presented and their basic operational characteristics are briefly discussed. Section III provides a more comprehensive analysis of the operating principles of each hybrid topology as well as the derivation of the rating relations. In Section IV the rating equations are used for analyzing and illustrating the PQ capabilities of the hybrid topologies. Section V presents an overall comparison of the studied topologies based on several criteria. In Section VI interesting observations regarding one of the topologies are briefly discussed. Finally, Section VII outlines the conclusions of this paper.

Note that part of this paper, related to the rating comparison of two of the topologies, has been accepted for publication in the 2016 8^{th} International Power Electronics and Motion Control Conference (IPEMC 2016—ECCE Asia) [23].

II. General Description of Hybrid Topologies

A. Hybrid Topologies With Voltage Injection

The hybrid topologies that exploit the FB arms for voltage injection are

- topology for series compensation with FB arms connected in series at the ac side of the LCC (SAC)—one arm per phase (see Fig. 1);
- topology for series compensation with FB arms connected in series at the dc side of the LCC (SDC)—two arms per phase (see Fig. 2).

The SAC topology shown in Fig. 1 is a variant of the ACC concept that is described in [6]. This topology relies on the injection of a controllable alternating voltage of the fundamental frequency V_{fa} in series with the grid voltage V_{sa}. This voltage injection allows the thyristors to be fired at negative firing angles α and the converter can commutate even under reduced grid voltage in case of faults. Although these features can be achieved with a passive capacitor, the issue of commutation failure [6] can be resolved only by the active capacitor. The series-coupling transformers of the ACC [6] can be eliminated by replacing the VSC by FB arms. However, the FB arm cannot handle active power and hence, the injected voltage V_{fa} and the LCC current I_{sa1} must be orthogonal, i.e., have a phase difference of $90°$.

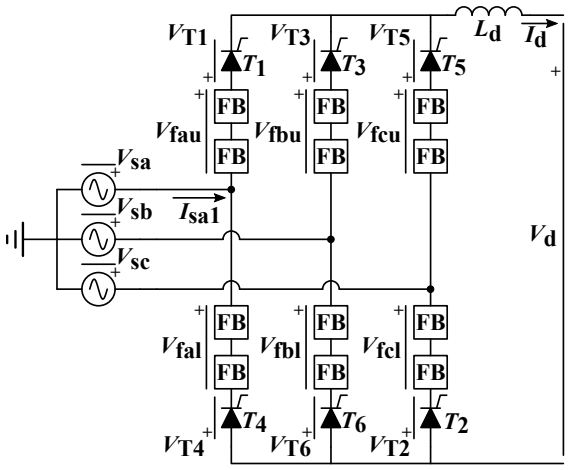

Fig. 2. SDC topology: LCC with FB arms connected in series at the dc side.

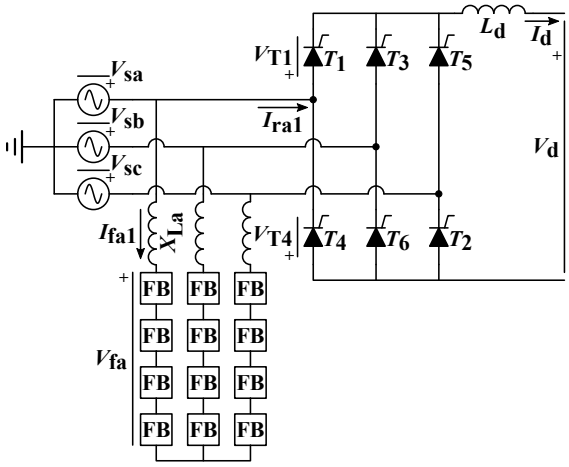

Fig. 3. PAC topology: LCC with an FB VSC connected in parallel at the ac side.

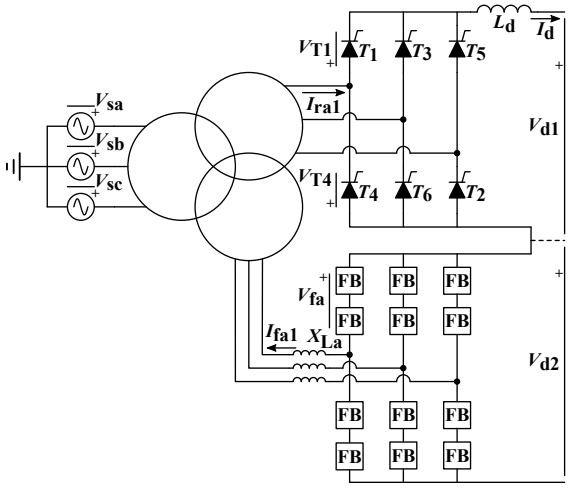

Fig. 4. SPM topology: LCC with an FB MMC connected in parallel at the ac and series at the dc side.

Another variant of series voltage injection is the SDC topology, shown in Fig. 2. In this topology the FB arms are connected at the dc side of the LCC. This means that the current through the FB cells is unidirectional and thus, these cells may be simplified by eliminating semiconductor switches that are only needed in case of bidirectional current. This idea is used in [25] for simplifying the half-bridge cell. Also for this converter, the orthogonality between the injected voltage $V_{\rm fa}$ and the LCC current $I_{\rm sa1}$ must be maintained.

A special characteristic of the SAC and SDC topologies is that the thyristors can be replaced by diodes provided that the FB arms have adequate voltage rating for blocking potential dc-faults [26].

B. Hybrid Topology With Current Injection

The topology of Fig. 3 relies on shunt current injection that is performed by connecting three FB arms (one per phase) in parallel at the ac side of the LCC. This hybrid topology is termed PAC, which stands for parallel compensation with FB arms connected in parallel at the ac side of the LCC. The reduced filtering requirements of the FB arms makes them favorable compared to a conventional two-level converter. As a matter of fact, the FB arm can be used for filtering the LCC current. Yet, this is not studied in this paper. Note that the operation of the FB arm is independent from the operation of the LCC. Thus, the FB arm can provide reactive-power support to the grid, even if the LCC is completely blocked. The main difference of the PAC compared to the SAC topology is that the commutation voltage cannot be changed by the FB arms, as this is always provided by the grid. Nevertheless, that the amplitude and phase angle of the fundamental grid current $I_{\rm sa1}$ can be controlled by the FB arms via the injection of an ac current of the fundamental frequency $I_{\rm fa1}$ that interacts with the LCC fundamental current $I_{\rm ra1}$. Finally, note that the orthogonality requirement between the injected current $I_{\rm fa1}$ and the converter bus voltage $V_{\rm fa}$ applies for the PAC, similarly to the series injection converters.

C. Hybrid Topology With Full-Bridge MMC

Finally, the hybrid topology that uses an FB MMC for handling both reactive and active power is termed series- and parallel-connected FB MMC at the dc and ac sides respectively (SPM) and is shown in Fig. 4. The orthogonality requirement does not apply to the SPM topology where the FB MMC can handle active power due to its connection with the dc link of the LCC, as shown in Fig. 4. Moreover, since the dc-link voltage of the FB MMC $V_{\rm d2}$ is controllable from rated positive $V_{\rm d2,r}$ to rated negative $-V_{\rm d2,r}$ value [26], the total dc-link voltage $V_{\rm d1}+V_{\rm d2}$ can be controlled by the FB MMC. In the special case that the rated dc-link voltage of the LCC $V_{\rm d1,r}$ is equal to $V_{\rm d2,r}$, the total dc-link voltage $V_{\rm d1}+V_{\rm d2}$ can be controlled exclusively by the FB MMC. In this way, for rectifier operation the LCC can be operated at minimum firing angle and the dc-link voltage can be controlled between the rated value $V_{\rm d1,r}+V_{\rm d2,r}$ and zero by varying the FB MMC voltage between $V_{\rm d2,r}$ and $-V_{\rm d2,r}$ respectively. As a result, the LCC is operated at a fixed point with minimum reactive-power consumption while the FB MMC is able to control the active power through the dc-link. Similarly, for inverter mode the LCC can be operated at minimum extinction angle that leads to minimization of reactive-power consumption. Furthermore, this minimum reactive power consumed by the LCC can be provided by the FB MMC if this is rated accordingly. Finally, note that this topology is similar to the 12-pulse LCC and thus, a transformer is needed for isolating the ac system from the dc link.

III. Operating Principles and Rating Comparison of the Considered Hybrid Topologies

In this section the operation of the hybrid topologies under consideration is described with the help of phasor diagrams. In addition, the main equations for dimensioning the FB arms of each hybrid topology are presented. These equations are used for estimating the rating of the FB arms for all hybrid topologies. In order to compare these ratings, a per-unit (p.u.) system is defined based on an LCC that is rated for apparent power equal to the product $V_{\rm d0}I_{\rm d}$, where $V_{\rm d0}$ is the dc-link voltage for firing angle $\alpha=0^\circ$ and $I_{\rm d}$ is the dc-link current. Based on this, the base voltage $V_{\rm base}$, current $I_{\rm base}$, power $S_{\rm base}$ and impedance $Z_{\rm base}$ of the p.u. system are defined as

$$I_{\rm base}=I_{\rm sa1,rms}=\frac{\sqrt{6}}{\pi}I_{\rm d} \tag{1}$$

$$V_{\rm base}=V_{\rm sa,rms}=\frac{\pi}{3\sqrt{6}}V_{\rm d0} \tag{2}$$

$$S_{\rm base}=3V_{\rm sa,rms}I_{\rm sa1,rms}=V_{\rm d0}I_{\rm d} \tag{3}$$

$$Z_{\rm base}=\frac{V_{\rm base}^2}{S_{\rm base}} \tag{4}$$

where $V_{\rm sa,rms}$ is the rms voltage and $I_{\rm sa,rms}$ the rms fundamental current at the ac bus of the aforementioned LCC. Note that (1) and (2) are fundamental relations of the LCC [27]. This definition of the p.u. system and the assumption that all hybrid topologies are rated for the same power transfer $V_{\rm d0}I_{\rm d}$ establish a fair base of comparison.

A. Hybrid Topologies With Voltage Injection

The phasor diagrams that visualize the concept of series compensation are presented in Fig. 5. The significance of the phasor diagram of Fig. 5 for the advanced commutation of the thyristors becomes more clear by considering the voltage seen by thyristor T_1 in the SAC topology. This voltage can be estimated by assuming that T_5 is conducting, which means that voltage $V_{\rm sc}-V_{\rm fc}$ appears at the cathode of T_1. By using the Kirchhoff's voltage law (KVL) in the loop formed by $V_{\rm sc}$, $V_{\rm sa}$, T_5 and T_1, the voltage $V_{\rm T1}$ at the terminals of T_1 for the SAC is given by

$$V_{\rm T1}=V_{\rm ma}-V_{\rm mc}=V_{\rm sa}-V_{\rm fa}-V_{\rm sc}+V_{\rm fc}=V_{\rm sac}-V_{\rm fac} \tag{5}$$

where $V_{\rm ma}$ and $V_{\rm mc}$ are the commutation voltages at the anodes of T_1 and T_5 (or at the midpoint of phase legs a and c respectively, $V_{\rm sac}$ and $V_{\rm fac}$ are the line-to-line grid and injected voltages. In case the injected voltages are zero, then $V_{\rm T1}$ is

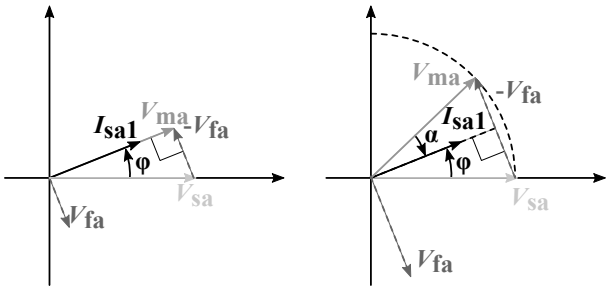

Fig. 5. SAC: Phasor diagrams for series compensation and for $\alpha = 0^\circ$ (left) and $\alpha > 0^\circ$ (right).

equal to the line-to-line grid voltage V_{sac}. This corresponds to the LCC case, where the commutation voltages V_{ma} and V_{mc} are equal to the grid voltages V_{sa} and V_{sc} respectively. Thus, the thyristor commutation relies solely on the grid voltages. However, by injecting the voltages V_{fa} and V_{fc} the commutation voltages can be phase shifted by the angle φ with respect to the grid voltages, as shown in Fig. 5 for phase a. As a result, the SAC topology can commutate at earlier time instants than the LCC, provided that the commutation voltage is leading the grid voltage. Similarly, the voltage V_{T1} at the terminals of T_1 for the SDC topology is given by

$$V_{\mathrm{T1}} = (V_{\mathrm{sa}} - V_{\mathrm{sc}}) + (V_{\mathrm{fau}} - V_{\mathrm{fcu}})\,. \tag{6}$$

By comparing (5) and (6) and considering that the injected voltages must be orthogonal to the corresponding line currents, it can be concluded that V_{fa} and V_{fc} of the SAC topology must be equal to $-V_{\mathrm{fau}}$ and V_{fcu} of the SDC topology. This implies that, for achieving the same commutation voltage, the rating of both the upper and lower FB arms of the SDC should be the same as that of a single arm of the SDC topology. This can be shown by considering that the voltage seen by T_4 of the SDC is expressed by

$$V_{\mathrm{T4}} = -\left(V_{\mathrm{sa}} - V_{\mathrm{sc}}\right) + \left(V_{\mathrm{fal}} - V_{\mathrm{fcl}}\right). \tag{7}$$

Equation (7) reveals that, if $V_{\mathrm{fal}} = -V_{\mathrm{fau}}$ and $V_{\mathrm{fcl}} = -V_{\mathrm{fcu}}$, then $V_{\mathrm{T4}} = -V_{\mathrm{T1}}$ for the of the SDC topology. This is valid by default for the of the SAC topology, since V_{fa} and V_{fc} are common for the thyristors of phase legs a and c respectively. Therefore, the SDC topology requires FB arms with double voltage rating compared to the SAC topology for achieving the same phase shift φ.

Note that, even though the phasor diagrams of Fig. 5 correspond to the SAC topology, the phasor diagram for SDC is similar based on the brief commutation analysis. Fig. 5 illustrates the injection of voltage V_{fa} in series with the grid voltage V_{sa}, which leads to the commutation voltage V_{ma}. For firing angle α equal to zero, the fundamental phase current I_{sa1} of the LCC is in phase with the commutation voltage V_{ma}, as depicted in the left-side diagram of Fig. 5. As a result, the phase difference φ of the fundamental current I_{sa1} and the grid voltage V_{sa} coincides with the phase difference of the commutation and grid voltages. Yet, this represents a specific case of operation of the SAC topology.

The operation of the SAC is more generally described by the right-side graph of Fig. 5, for which $\alpha \neq 0^\circ$. The firing angle α in this graph introduces a phase difference between the commutation voltage V_{ma} and the fundamental current I_{sa1}. This is analogous to the conventional LCC, for which the firing angle introduces a phase difference between the fundamental current I_{sa1} and the grid voltage V_{sa} that is also the commutation voltage. As previously mentioned, the injected voltage V_{fa} and the fundamental current I_{sa1}, flowing through the FB arm of phase a, must be orthogonal and thus, phasors V_{ma}, V_{fa}, and I_{sa1} must form a right triangle. The same applies for the phasors V_{sa}, V_{fa}, and I_{sa1}. By using the common edge of these triangles, the relationship between the commutation voltage V_{ma} and the grid voltage V_{sa} can be expressed as

$$\hat{V}_{\mathrm{m}a} = \hat{V}_{\mathrm{sa}} \frac{\cos\varphi}{\cos\alpha} \tag{8}$$

where $\hat{V}_{ca}$ and $\hat{V}_{\mathrm{s}a}$ are the amplitudes of the commutation and grid voltage respectively and φ the power angle.

The relation that yields the required injected voltage V_{fa} for achieving a specific power angle φ can be derived by considering the orthogonality requirement between I_{sa} and V_{fa}, as shown in [23], and is as follows

$$\hat{V}_{\mathrm{fa}} = \hat{V}_{\mathrm{sa}} \frac{\sin\left(\varphi + \alpha\right)}{\cos\alpha}. \tag{9}$$

By using (9), the required voltage rating of each FB arm in the SAC topology can be estimated as a function of φ. The results are shown for various firing angles of the LCC in Fig. 8.

Since the current rating of each FB arm should be equal to the fundamental current of the LCC, Fig. 8 indirectly illustrates the required apparent power of each arm. As expected, the required apparent power increases with increasing power angle φ and with increasing firing angle α, due to the increased reactive-power demand.

The voltage and current rating of each FB arm of the SDC is the same as for the SAC. Yet, for operating both hybrid converters in the same way, six FB arms are required in total for the SDC, instead of three for the SAC. However, since the FB arms are connected in series with each thyristor valve, the voltage stress can be shared. This voltage stress should be equal to the line-to-line voltage $\hat{V}_{\mathrm{ll}} = \sqrt{2}V_{\mathrm{ll,rms}}$, as for a thyristor valve of an LCC. This can be expressed as

$$\hat{V}_{\mathrm{th}} + \hat{V}_{\mathrm{fbar}} = \hat{V}_{\mathrm{ll}} \tag{10}$$

where $\hat{V}_{\mathrm{th}}$ and $\hat{V}_{\mathrm{fbar}}$ are the blocking voltage of each thyristor valve and the corresponding FB arm respectively. If the FB arm handles just a portion k_{vb} of the total voltage stress $\hat{V}_{\mathrm{ll}}$, (10) can be rewritten as

$$\hat{V}_{\mathrm{th}} + k_{\mathrm{vb}}\hat{V}_{\mathrm{ll}} = \hat{V}_{\mathrm{ll}} \Rightarrow \hat{V}_{\mathrm{th}} = \left(1 - k_{\mathrm{vb}}\right)\hat{V}_{\mathrm{ll}} \tag{11}$$

where k_{vb} represents the ratio of the arm's blocking voltage and the total voltage stress $\hat{V}_{\mathrm{ll}}$. Furthermore, (11) shows that the required blocking voltage of the thyristor valve decreases with increasing blocking voltage (or voltage rating) of the FB arm. Hence, the increasing voltage rating shown in Fig. 8

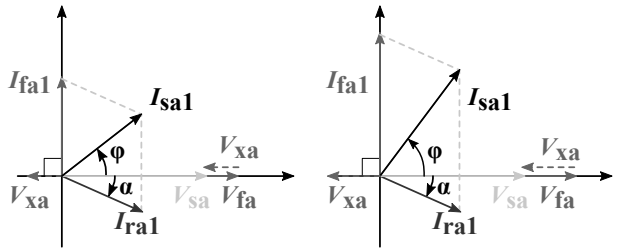

Fig. 6. PAC: Phasor diagram for parallel compensation and for two different values of φ.

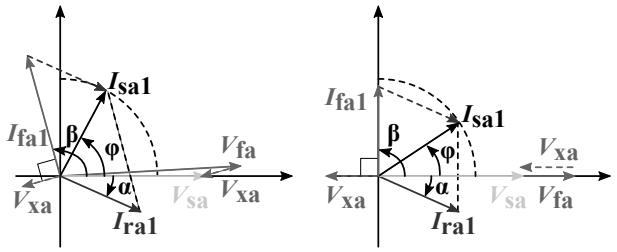

Fig. 7. SPM: Phasor diagram for two different values of φ.

would lead to a decreasing blocking voltage of the thyristor valves of the SDC.

B. Hybrid Topology With Current Injection

The operation of the PAC topology is based on current injection for compensating the reactive power of the LCC, as illustrated by the phasor diagrams in Fig. 6. These phasor diagrams show that the injected current $I_{\rm fa1}$ interacts with the current of the LCC $I_{\rm ra1}$ so that the grid current $I_{\rm sa1}$ is regulated in terms of both amplitude and phase angle. Note that the main differences of the PAC topology from the SAC topology are that the commutation voltage coincides with the grid voltage, similarly to a conventional LCC, and that the grid current does not coincide with the LCC current $I_{\rm ra1}$. These differences can be observed also by comparing Fig. 1 and Fig. 3.

In addition, Fig. 3 shows that each FB arm of the PAC topology is connected to the ac-bus of the LCC via a coupling inductance, which may represent a transformer leakage inductance, in case a transformer is used for the connection. Essentially it is the voltage drop across this coupling inductance $V_{\rm xa}$ that defines the amplitude of the injected current $I_{\rm fa1}$. Thus, the FB arm should be able to generate a voltage $V_{\rm fa}$ that can create a suitable voltage drop $V_{\rm xa}$ for achieving a specific power angle φ. Fig. 6 shows both of these voltages as well as their orthogonality relationship with the injected current $I_{\rm fa1}$. The orthogonality requirement ensures that the FB arms neither absorb nor inject any active power from or to the grid and in this case implies that $V_{\rm fa}$ must be in phase with the grid voltage $V_{\rm sa}$. Thus, the injection of $I_{\rm fa1}$ impacts only the reactive component of the grid current $I_{\rm sa1}$, which allows the PAC topology to independently control active and reactive power.

However, the extent that reactive power can be controlled is dependent on the current rating of the FB arm. This required current rating for achieving a specific power angle φ can be derived by considering the components of current phasors in Fig. 6, as shown in [23], and is given by

$$\hat{I}_{\rm fa1} = \hat{I}_{\rm ra1}\cos\alpha\tan\varphi + \hat{I}_{\rm ra1}\sin\alpha \tag{12}$$

where $\hat{I}_{\rm ra1}$ is the amplitude of the fundamental current drawn by the LCC. In addition, for being able to inject the current defined by (12), the FB arm needs to have a voltage rating $\hat{V}_{\rm fa}$ that is given by

$$\hat{V}_{\rm fa} = \hat{V}_{\rm sa} + \hat{V}_{\rm xa} = \hat{V}_{\rm sa} + \hat{I}_{\rm fa}x_{\rm La} \tag{13}$$

where $\hat{V}_{\rm sa}$ and $\hat{V}_{\rm xa}$ are the amplitudes of the grid voltage and the voltage drop on the coupling inductance $x_{\rm La}$ respectively. By using (12), (13) and assuming a coupling inductance of 0.12 p.u., the required current and voltage ratings of each FB arm are estimated as a function of φ. The results are shown in Fig. 9 for various firing angles.

C. Hybrid Topology With Full-Bridge MMC

Finally, the SPM topology can be considered as an extension of the PAC topology toward enabling the FB arms to handle also active power. This extension is achieved by modifying the three FB arms to an FB MMC and connecting its dc link in series with that of the LCC. The FB MMC is able to regulate the dc-link voltage, and hence the power, of the SPM topology. Such operation could not be achieved with other VSCs, such as two- or three-level VSCs, or even the half-bridge MMC. The control of active and reactive power by the FB MMC of the SPM topology is illustrated in the phasor diagrams of Fig. 7.

Fig. 7 shows the voltage $V_{\rm fa}$ and current $I_{\rm fa1}$ phasors of the FB MMC for a case where this converter handles either both active and reactive power (left-hand diagram) or only reactive power (right-hand diagram). Similarly to the PAC topology, the voltage drop $V_{\rm xa}$ across the coupling inductance $x_{\rm La}$ defines the current $I_{\rm fa1}$ that is injected by the FB MMC. In both phasor diagrams of Fig. 7, note the introduction of angle β, which is the phase difference between the injected current $I_{\rm fa1}$ and the grid voltage $V_{\rm sa}$. Angle β defines the power factor of the FB MMC.

For facilitating the analysis and discussion, the complementary voltage ratios $k_{\rm v}$ and $k_{\rm s}$ are defined as

$$k_{\rm v} = \frac{V_{\rm d2,r}}{V_{\rm d,hyb}} \Rightarrow k_{\rm s} = 1 - k_{\rm v} = \frac{V_{\rm d1,r}}{V_{\rm d,hyb}} \tag{14}$$

where $k_{\rm v}$ and $k_{\rm s}$ indicate the portion of the dc-link voltage that is handled by the FB MMC and the LCC respectively, $V_{\rm d1,r}$ and $V_{\rm d2,r}$ are the rated dc-link voltages of the LCC (i.e., for $\alpha = 0°$) and FB MMC respectively, while $V_{\rm d,hyb}$ is their sum. For ensuring that the dc-link power rating of the SPM is the same as for the other hybrid converters, $V_{\rm d,hyb}$ is defined based on the p.u. base values as follows

$$V_{\rm d,hyb} = V_{\rm d0} = \frac{3\sqrt{3}}{\pi}\hat{V}_{\rm sa}. \tag{15}$$

Based on (14) and (15), the voltage at the ac bus of the LCC should be scaled according to k_s (or k_v), since $V_\mathrm{d1,r}$ represents the dc-link voltage of the LCC for $\alpha = 0°$. If $\hat{V}_\mathrm{sa,s}$ is defined as the voltage at the ac bus of the LCC, its relation with the p.u. base voltage $\hat{V}_\mathrm{sa}$ can be derived by combining (14) and (15) as follows

$$V_\mathrm{d1,r} = \frac{3\sqrt{3}}{\pi}\hat{V}_\mathrm{sa,s} \Rightarrow \hat{V}_\mathrm{sa,s} = \frac{\pi}{3\sqrt{3}}\left(1-k_\mathrm{v}\right)V_\mathrm{d,hyb} \Rightarrow \hat{V}_\mathrm{sa,s} = \left(1-k_\mathrm{v}\right)\hat{V}_\mathrm{sa} = k_\mathrm{s}\hat{V}_\mathrm{sa}. \tag{16}$$

where $\hat{V}_\mathrm{sa}$ is the voltage at the primary side and $\hat{V}_\mathrm{sa,s}$ is the voltage at the secondary side of the transformer (i.e., at the ac bus of the LCC) of the SPM. Equation (16) is important, because $\hat{V}_\mathrm{sa,s}$ is used as a base for dimensioning the FB MMC. More specifically, the required voltage rating of the FB MMC for achieving a specific I_fa1 can be given by

$$I_\mathrm{fa1} = \frac{V_\mathrm{sa,s} - V_\mathrm{fa}}{x_\mathrm{La}} \Rightarrow V_\mathrm{fa} = \left(1-k_\mathrm{v}\right)V_\mathrm{sa} - I_\mathrm{fa1}x_\mathrm{La} \tag{17}$$

where I_fa1 represents the required current rating of the FB MMC for achieving a specific φ for the SPM. This current rating can be estimated from the phasor diagrams of Fig. 7, by summing the x- and y-axis components of the grid current I_sa1 and the LCC current I_ra1 as follows:

$$I_\mathrm{fa1,x} = I_\mathrm{sa1,x} - I_\mathrm{ra1,x} \Rightarrow \hat{I}_\mathrm{fa1}\cos\beta = \hat{I}_\mathrm{sa1}\cos\varphi - \hat{I}_\mathrm{ra1}\cos\alpha \tag{18}$$

$$I_\mathrm{fa1,y} = I_\mathrm{sa1,y} - I_\mathrm{ra1,y} \Rightarrow \hat{I}_\mathrm{fa1}\sin\beta = \hat{I}_\mathrm{sa1}\sin\varphi + \hat{I}_\mathrm{ra1}\sin\alpha. \tag{19}$$

The amplitude $\hat{I}_\mathrm{fa1}$ can be estimated by summing the squares of (18) and (19). By considering also the trigonometric identity $\cos^2\delta + \sin^2\delta = 1$, it follows that

$$\hat{I}_\mathrm{fa1}^2 = \hat{I}_\mathrm{sa1}^2 + \hat{I}_\mathrm{ra1}^2 - 2\hat{I}_\mathrm{sa1}\hat{I}_\mathrm{ra1}\left(\cos\varphi\cos\alpha - \sin\varphi\sin\alpha\right). \tag{20}$$

Finally, $\hat{I}_\mathrm{fa1}$ can be derived by rewriting (20) and β by rewriting (18) as follows

$$\hat{I}_\mathrm{fa1} = \sqrt{\hat{I}_\mathrm{sa1}^2 + \hat{I}_\mathrm{ra1}^2 - 2\hat{I}_\mathrm{sa1}\hat{I}_\mathrm{ra1}\cos\left(\varphi+\alpha\right)} \tag{21}$$

$$\beta = \arcsin\left(\frac{\hat{I}_\mathrm{sa1}\sin\varphi + \hat{I}_\mathrm{ra1}\sin\alpha}{\hat{I}_\mathrm{fa1}}\right). \tag{22}$$

At this point, it is convenient to substitute k_s in (21) and (22). Thus, by considering that $V_\mathrm{d1,r}I_\mathrm{d} = (3/2)\hat{V}_\mathrm{sa,s}\hat{I}_\mathrm{ra1}$ and $(V_\mathrm{d1,r}+V_\mathrm{d2,r})I_\mathrm{d} = (3/2)\hat{V}_\mathrm{sa,s}\hat{I}_\mathrm{sa1}$, the fundamental current of the LCC (I_ra1) can be expressed in terms of k_s as

$$k_\mathrm{s} = \frac{V_\mathrm{d1,r}}{V_\mathrm{d1,r}+V_\mathrm{d2,r}} = \frac{\hat{I}_\mathrm{ra1}}{\hat{I}_\mathrm{sa1}} \tag{23}$$

Based on (23), both (21) and (22) can be transformed in

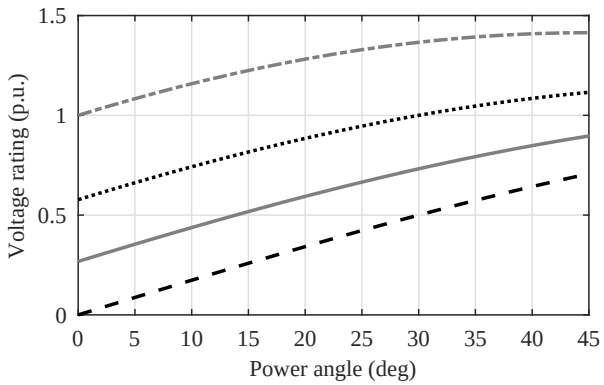

Fig. 8. SAC: Voltage rating of each FB arm versus the power angle φ, for firing angles $\alpha = 0°$ (dashed line) $\alpha = 15°$ (solid gray line), $\alpha = 30°$ (dotted line), $\alpha = 45°$ (two-dashed gray line).

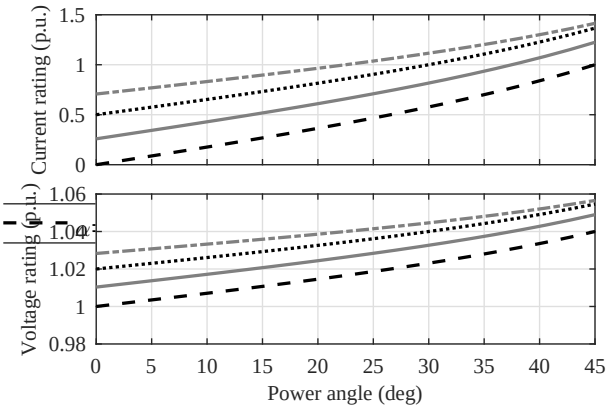

Fig. 9. PAC: Current (upper) and voltage (lower) rating (rms) of each FB arm versus the power angle φ, for firing angles $\alpha = 0°$ (dashed line) $\alpha = 15°$ (solid gray line), $\alpha = 30°$ (dotted line), $\alpha = 45°$ (two-dashed gray line).

$$\hat{I}_\mathrm{fa1} = \hat{I}_\mathrm{sa1}\sqrt{1 + k_\mathrm{s}^2 - 2k_\mathrm{s}\cos\left(\varphi+\alpha\right)} \tag{24}$$

$$\beta = \arcsin\left(\hat{I}_\mathrm{sa1}\frac{\sin\varphi + k_\mathrm{s}\sin\alpha}{\hat{I}_\mathrm{fa1}}\right). \tag{25}$$

where β is the phase difference of I_fa1 and V_sa, hence, representing the power angle of the FB MMC.

The voltage rating of the FB MMC can now be estimated by analyzing (17) in the x- and y-axis components, following a similar approach as for I_fa1. Note that V_sa can be represented simply by its amplitude, since it is considered the reference with argument equal to zero. Furthermore, from the phasor diagrams of Fig. 7 it can be seen that the argument of $V_\mathrm{xa} = I_\mathrm{fa1}x_\mathrm{La}$ is $\gamma = (\beta+\pi/2)$, where $(\pi/2)$ is the phase difference of V_xa from I_fa1. Based on these definitions, the amplitude and argument of V_fa can be expressed as

$$\hat{V}_\mathrm{fa} = \sqrt{\left(k_\mathrm{s}\hat{V}_\mathrm{sa} - \hat{I}_\mathrm{fa1}x_\mathrm{La}\cos\gamma\right)^2 + \left(\hat{I}_\mathrm{fa1}x_\mathrm{La}\sin\gamma\right)^2} \tag{26}$$

Finally, by using (24)-(26), the required ac-side current and voltage ratings of the FB MMC in the SPM topology are estimated as a function of the power angle φ. However, the

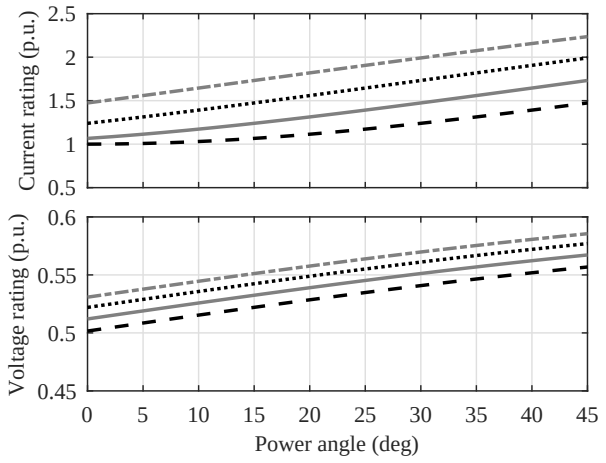

Fig. 10. SPM: Current (upper) and voltage (lower) rating (rms) of the FB MMC versus the power angle φ, for firing angles $\alpha = 0°$ (dashed line) $\alpha = 15°$ (solid gray line), $\alpha = 30°$ (dotted line), $\alpha = 45°$ (two-dashed gray line).

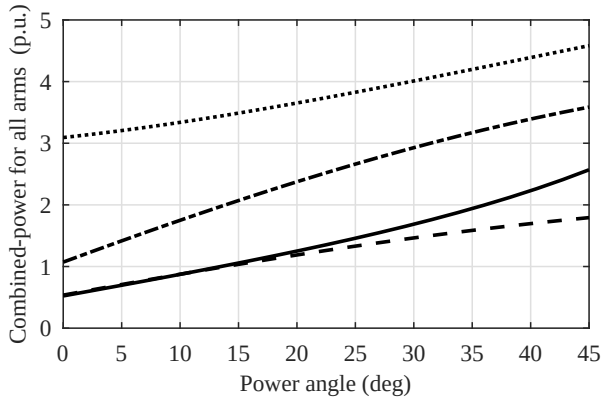

Fig. 11. Combined power rating of all arms for the SAC (dashed line), the SDC (two-dashed line), the PAC (solid line) and the SPM (dotted line) topologies versus the power angle φ for firing angle $\alpha = 15°$.

amplitude of the grid current I_{sa1} and the voltage ratio k_{s} must be defined. For this analysis, the dc-link voltage ratios are selected as $k_{\mathrm{s}} = 0.5 = k_{\mathrm{v}}$, which represents the special case of operation of the SPM that was explained before. According to this selection, the LCC can be operated at minimum firing angle and the dc-link voltage, and thus power, can be fully controlled by the FB MMC. Moreover, the amplitude of the grid current $\hat{I}_{\mathrm{sa1}}$ is set to $1/\sqrt{2}$ p.u. for all power angle φ. Thus, the phasor I_{sa1} is moved along the dashed curve shown in Fig. 7, depending on the desired value of φ. The results are depicted for various firing angles of the LCC in Fig. 10. Nevertheless, each of the six FB arms of the SPM should be dimensioned according to $\hat{V}_{\mathrm{fa}}$, $\hat{I}_{\mathrm{fa1}}$, as well as the dc-link voltage V_{d2} and current I_{d} as follows [19], [28]

$$\hat{V}_{\mathrm{arm}} = \hat{V}_{\mathrm{fa}} + \frac{V_{\mathrm{d2}}}{2},\ \hat{I}_{\mathrm{arm}} = \frac{\hat{I}_{\mathrm{fa1}}}{2} + \frac{I_{\mathrm{d}}}{3} \tag{27}$$

where $\hat{V}_{\mathrm{arm}}$ and $\hat{I}_{\mathrm{arm}}$ are the total voltage and current ratings of each FB arm.

D. Rating Comparison of the Considered Hybrid Topologies

A comparison of the considered hybrid topologies can be performed after estimating the required voltage and current ratings for the FB arms. This comparison is performed by assuming a firing angle $\alpha = 15°$ for the LCC of all hybrid topologies. This value of α is chosen because it represents the minimum firing angle at which LCCs are typically operated [27, Ch. 3]. Moreover, since the arms of the SPM are rated a bit differently than the rest of the topologies, the combined-power rating of all arms of each topology is used as a base for the comparison. This rating (S_{comb}) is defined as [28]

$$S_{\mathrm{comb}} = N_{\mathrm{a}} \hat{V}_{\mathrm{arm}} \hat{I}_{\mathrm{arm}} \tag{28}$$

where N_{a} is the total number of arms per hybrid topology. The combined power rating S_{comb} is just the product of the voltage $\hat{V}_{\mathrm{arm}}$ and current ratings $\hat{I}_{\mathrm{arm}}$ of each FB arm of a hybrid converter, multiplied by the number of arms N_{a} for the same converter. As such, S_{comb} simply represents the power handling capability of all FB arms. Hence, normalizing the total S_{comb} by the power handled by the corresponding converter serves as a utilization index of the FB arms. Moreover, the variables N_{a}, $\hat{V}_{\mathrm{arm}}$ and $\hat{I}_{\mathrm{arm}}$ for each topology are defined as follows:

- SAC: $N_{\mathrm{a}} = 3$, $\hat{V}_{\mathrm{arm}} = \hat{V}_{\mathrm{fa}}$, $\hat{I}_{\mathrm{arm}} = \hat{I}_{\mathrm{fa1}}$;
- SDC: $N_{\mathrm{a}} = 6$, $\hat{V}_{\mathrm{arm}} = \hat{V}_{\mathrm{fa}}$, $\hat{I}_{\mathrm{arm}} = \hat{I}_{\mathrm{fa1}}$;
- PAC: $N_{\mathrm{a}} = 3$, $\hat{V}_{\mathrm{arm}} = \hat{V}_{\mathrm{fa}}$, $\hat{I}_{\mathrm{arm}} = \hat{I}_{\mathrm{fa1}}$;
- SPM: $N_{\mathrm{a}} = 6$, $\hat{V}_{\mathrm{arm}}$, $\hat{I}_{\mathrm{arm}}$ according to (27).

Finally, the combined-power rating of all arms is shown for all topologies in Fig. 11, which shows that the minimum combined-power rating is achieved with the SAC. Similar rating is required for the PAC for power angles up to 20°, whereas beyond this value the rating of the SAC scales better. However, the operation of the PAC is not limited by the thyristor voltage stress and thus this topology can be controlled more flexibly than the SAC. Moreover, the rating of the SDC is double that of the SAC. However, the advantage of this topology over the SAC is that its arms contribute to lowering the rating of the LCC, as indicated by (11). The same is valid for the SPM, as shown by (14). The additional benefit of the SPM is that the LCC is always operated at minimum α, which leads to minimization of reactive-power consumption and harmonics. Moreover, the dc-link power can be fully controlled by the FB MMC and thus the SPM is more flexible in terms of control. In summary, even though the SAC is the best option in terms of rating, this comparison does not allow for solid conclusions. Thus, more criteria should be added for a more complete comparison. The PQ capability can serve as an interesting criterion, as this is an important limitation of the conventional LCC. Hence, the PQ capability of all hybrid topologies is investigated and compared in Section IV.

IV. PQ Capability Analysis and Comparison of the Considered Hybrid Topologies

In this section the PQ capability of the studied hybrid topologies is analyzed based on the corresponding phasor diagrams and rating equations. The main LCC characteristic

TABLE I
ESTIMATED REQUIRED RMS RATINGS OF FB ARMS FOR ACHIEVING $\varphi = 45^\circ$ WHILE $\alpha = 15^\circ$.

Topology	V_{chl} (p.u.)	I_{chl} (p.u.)	S_{comb} (p.u.)	S_{LCC} (p.u.)
SAC	0.9	1	1.8	1
SDC	0.9	1	3.6	0.48
PAC	1.05	1.22	2.6	1
SPM	0.57	1.7	4.6	0.5

that is impacted by the introduction of FB arms is the active-reactive (PQ) capability. Since the active and reactive power of the LCC cannot be controlled independently and the LCC reactive-power consumption is significant, the introduction of the FB arms in the hybrid topologies may serve two purposes:

1) compensate the reactive-power consumption of the LCC;
2) partially decouple the active- and reactive-power control of the LCC.

A. Hybrid Topologies With Voltage Injection

The concept of voltage injection is illustrated in the phasor diagrams of Fig. 5. The impact of voltage injection on the dc-link voltage of the SAC topology is now studied. For a conventional LCC, the dc-link voltage V_{d} is a function of the amplitude of the commutation voltage $\hat{V}_{\mathrm{ca}}$ and the firing angle α, as described by

$$V_{\mathrm{d}} = \frac{3\sqrt{3}}{\pi}\hat{V}_{\mathrm{ca}}\cos\alpha. \tag{29}$$

The commutation voltage of a conventional LCC coincides with the grid voltage, if the small transformer leakage inductance that is interposed between the grid and the LCC terminals is neglected. Thus, since the grid voltage is constant under normal operation, from (29) follows that the dc-link voltage of a conventional LCC depends only on the firing angle α. In contrast, the commutation voltage of the SAC topology depends on the voltage that is injected for achieving a specific power angle φ, as described by (8). Therefore, the expression of the dc-link voltage for the SAC can be derived by substituting (8) in (29), which yields

$$V_{\mathrm{d}} = \frac{3\sqrt{3}}{\pi}\hat{V}_{\mathrm{sa}}\cos\varphi. \tag{30}$$

Equation (30) shows that the dc-link voltage of the SAC topology is no longer dependent on the firing angle α, but on the power angle φ instead. However, (29) and (30) are analogous and imply that the dc-link voltage is always dependent on the phase difference between the grid voltage and the fundamental current flowing through the LCC. Since this phase difference defines both active and reactive power at the same time, the independent control of active and reactive power is not possible. Moreover, (30) could be assumed to represent the dc-link voltage of a hypothetical LCC, where $\hat{V}_{\mathrm{sa}}$ represents the commutation voltage and φ respresents the "firing angle." Based on this, the operating point of the SAC can be described by

$$\begin{aligned} S_{\mathrm{hyb}}^2 &= P_{\mathrm{hyb}}^2 + Q_{\mathrm{hyb}}^2 \\ &= \left(\frac{3}{2}\hat{V}_{\mathrm{sa}}\hat{I}_{\mathrm{sa1}}\cos\varphi\right)^2 + \left(\frac{3}{2}\hat{V}_{\mathrm{sa}}\hat{I}_{\mathrm{sa1}}\sin\varphi\right)^2. \end{aligned} \tag{31}$$

Since the injection of V_{fa} impacts the amplitude of the commutation voltage $\hat{V}_{\mathrm{ca}}$, φ is affected by the injected voltage for a certain α, based on (8). Thus, from (31) it follows that the injected voltage modifies both the active (P_{hyb}) and reactive (Q_{hyb}) power of the SAC.

B. Hybrid Topology With Current Injection

The operation of the PAC topology is based on current injection for compensating the reactive power of the LCC, as illustrated by the phasor diagrams in Fig. 6. These phasor diagrams show that the injected current I_{fa1} interacts with the current of the LCC I_{ra1} so that the grid current I_{sa1} is regulated in terms of both amplitude and phase angle. Note that the main differences of the PAC topology from the SAC topology are that the grid current does not coincide with the LCC current I_{ra1} and the commutation voltage coincides with the grid voltage, similarly to a conventional LCC. Therefore, current injection does not impact the dc-link voltage, in contrast to voltage injection. These differences can be observed also by comparing Fig. 5 and Fig. 6.

The relation that describes the PQ capability of the PAC can be derived by expressing the amplitude of the grid current $\hat{I}_{\mathrm{sa1}}$ with respect to the current injected by the FB arm $\hat{I}_{\mathrm{fa1}}$ and the current of the LCC $\hat{I}_{\mathrm{ra1}}$. Hence, by considering the components of the respective current phasors in Fig. 6, the amplitude $\hat{I}_{\mathrm{sa1}}$ can be expressed by

$$\hat{I}_{\mathrm{sa1}} = \sqrt{(\hat{I}_{\mathrm{ra1}}\cos\alpha)^2 + (\hat{I}_{\mathrm{fa1}}\sin\frac{\pi}{2} - \hat{I}_{\mathrm{ra1}}\sin\alpha)^2}. \tag{32}$$

Moreover, by using (32) it follows that

$$\begin{aligned} S_{\mathrm{hyb}}^2 = P_{\mathrm{hyb}}^2 + Q_{\mathrm{hyb}}^2 &= \left(\frac{3}{2}\hat{V}_{\mathrm{sa}}\hat{I}_{\mathrm{sa1}}\right)^2 = \left(\frac{3}{2}\hat{V}_{\mathrm{sa}}\right)^2\hat{I}_{\mathrm{sa1}}^2 \\ &= \left(\frac{3}{2}\hat{V}_{\mathrm{sa}}\hat{I}_{\mathrm{ra1}}\cos\alpha\right)^2 + \left(\frac{3}{2}\hat{V}_{\mathrm{sa}}\hat{I}_{\mathrm{fa1}} - \frac{3}{2}\hat{V}_{\mathrm{sa}}\hat{I}_{\mathrm{ra1}}\sin\alpha\right)^2 \\ &= P_{\mathrm{LCC}}^2 + \left(Q_{\mathrm{fa}} - Q_{\mathrm{LCC}}\right)^2. \end{aligned} \tag{33}$$

where Q_{fa} is the reactive power injected by the FB arms of the PAC topology. This reactive power can be regulated by varying the amplitude of the injected current $\hat{I}_{\mathrm{fa1}}$. The injected current I_{fa1} modifies the amplitude and phase angle of the current seen by the grid I_{sa1} without impact on the current of the LCC I_{ra1}. Therefore, the reactive power (Q_{hyb}) of the PAC topology can be modified without imposing any change to the firing angle and thus, the active power of the LCC. Yet, for a given power rating of the FB converter, the maximum reactive power that could be generated by the hybrid PAC topology is dependent on the firing angle of the LCC.

C. Hybrid Topology With Full-Bridge MMC

Finally, the SPM topology can be considered as an extension of the PAC topology towards enabling the FB arms to handle also active power. This extension is achieved by introducing a FB MMC and connecting its dc link in series with that of the LCC.

Fig. 7 shows the voltage $V_{\rm fa}$ and current $I_{\rm fa1}$ phasors of the FB MMC for a case where this converter handles either both active and reactive power (left-hand diagram) or only reactive power (right-hand diagram). Similarly to the PAC topology, the voltage drop $V_{\rm xa}$ across the coupling inductance $x_{\rm La}$ defines the current $I_{\rm fa1}$ that is injected by the FB MMC. In both phasor diagrams of Fig. 7, note the introduction of angle β that is the phase difference between the injected current $I_{\rm fa1}$ and the grid voltage $V_{\rm sa}$. Angle β defines the power factor of the FB MMC.

The FB MMC must be controlled in such a way that power balance between the ac and dc sides is ensured, i.e.,

$$V_{\rm d2} I_{\rm d} = \frac{3}{2}\hat{V}_{\rm sa}\hat{I}_{\rm fa1}\cos\beta. \tag{34}$$

Due to the current-source behavior of the LCC, the dc-link current $I_{\rm d}$ in (34) is constant. Therefore, the dc-link power can be controlled only by means of the dc-link voltage $V_{\rm d2}$, which should be controlled so that

$$V_{\rm d2} = \frac{3\hat{V}_{\rm sa}\hat{I}_{\rm fa1}}{2I_{\rm d}}\cos\beta. \tag{35}$$

Equation (35) shows that $V_{\rm d2}$ should be controlled according to the power angle β and the amplitude of the injected current $\hat{I}_{\rm fa1}$ of the FB MMC. In the case where the FB MMC is supplying only reactive power and thus, $\beta = 90^\circ$, $V_{\rm d2}$ must be set to zero, while $\hat{I}_{\rm fa1}$ can be altered arbitrarily. Nevertheless, when $\beta < 90^\circ$, $V_{\rm d2}$ must be positive and changed according to $\hat{I}_{\rm fa1}$. The same applies when $\beta > 90^\circ$ but $V_{\rm d2}$ must be negative instead.

By considering the specific cases where $\beta = 0^\circ$ or $\beta = 180^\circ$, (35) shows that $V_{\rm d2}$ can be controlled between 0 and its rated positive value $V_{\rm d2,r}$ or between 0 and its rated negative value $-V_{\rm d2,r}$. Therefore, by selecting a direct-voltage ratio $k_{\rm v}$ of 0.5, the dc-link voltage of the SPM can be fully controlled by the FB MMC. Thus, the LCC can always be operated at the firing angle α that corresponds to the minimum reactive-power consumption. However, for compensating this reactive power, the FB MMC should be oversized with respect to its active-power transfer capability $P_{\rm d,VSC} = V_{\rm d2,r} I_{\rm d}$.

In order to define the relationship between active and reactive power of the SPM, a similar process as for the PAC topology is followed. Firstly, by summing the squares of the current phasor components in (18) and (19), the amplitude of the grid current can be expressed as follows:

$$\begin{aligned}\hat{I}_{\rm sa1}^2 = (\hat{I}_{\rm fa1}\cos\beta + \hat{I}_{\rm ra1}\cos\alpha)^2 + \\ (\hat{I}_{\rm fa1}\sin\beta - \hat{I}_{\rm ra1}\sin\alpha)^2.\end{aligned} \tag{36}$$

Thus, by considering (36) it follows that

$$\begin{aligned} S_{\rm hyb}^2 =& P_{\rm hyb}^2 + Q_{\rm hyb}^2 = \left(\frac{3}{2}\hat{V}_{\rm sa}\hat{I}_{\rm sa1}\right)^2 \\ =& \left(\frac{3}{2}\hat{V}_{\rm sa}\hat{I}_{\rm fa1}\cos\beta + \frac{3}{2}\hat{V}_{\rm sa}\hat{I}_{\rm ra1}\cos\alpha\right)^2 \\ &+ \left(\frac{3}{2}\hat{V}_{\rm sa}\hat{I}_{\rm fa1}\sin\beta - \frac{3}{2}\hat{V}_{\rm sa}\hat{I}_{\rm ra1}\sin\alpha\right)^2 \\ =& \left(P_{\rm fa} + P_{\rm LCC}\right)^2 + \left(Q_{\rm fa} - Q_{\rm LCC}\right)^2. \end{aligned} \tag{37}$$

In general, (37) is similar to (33) but extended to include the term $P_{\rm fa}$ that represents the active power of the FB MMC. This term implies that the FB MMC may be used to alter the active power ($P_{\rm hyb}$) of the hybrid SPM topology, unlike in the case of the PAC topology. Moreover, (37) shows that, unlike the PAC topology, both active ($P_{\rm hyb}$) and reactive ($Q_{\rm hyb}$) power of the SPM topology can be modified without altering the operating point of the LCC. More specifically, the LCC can operate at a fixed firing angle while the FB MMC can be controlled to generate or consume active or reactive power and thus, modify the operating point of the SPM topology. Based on this, it is possible for the LCC to supply active power to the dc-link while the FB MMC is absorbing active power from the dc-link and thus, counteracting the LCC. As a result, the dc-link power can be zero even if the LCC is operating as rectifier at minimum firing angle, which corresponds to maximum active-power transfer from the LCC to the dc-link. In such case, the dc-link voltage of the LCC is at maximum value, while the dc-link voltage of the FB MMC must be at the same value but with opposite sign. Hence, the FB MMC should have adequate voltage rating, which is ensured by $k_{\rm v} \geq 0.5$.

D. PQ Capability Comparison of the Considered Hybrid Topologies

The PQ capability is illustrated by the PQ curves of each hybrid converter, which are presented in Fig. 12. Fig. 12 shows the PQ curve of the LCC represented by the solid line, the extension of the PQ curve that is achieved by the FB arms represented by the light gray line/area and the ideal PQ curve represented by the dashed gray line. Note that the ideal curve represents the boundary of the PQ curve that could be achieved by using a VSC with apparent-power rating equal to the p.u. base $S_{\rm base}$. In this way, Fig. 12 illustrates how closely the PQ curve of each hybrid converter approximates that of a VSC. The PQ curve of the LCC is located in the region of inductive reactive power, which is defined as negative in this paper. Moreover, the FB arms enable the extension of the PQ curve in the region of capacitive reactive power, which is defined as positive in this paper. Note that the PQ curves of each hybrid topology were generated by considering FB arms that are rated for achieving a power angle $\varphi = 45^\circ$ while the LCC is operating at a firing angle of $\alpha = 15^\circ$. The reason for focusing on $\varphi = 45^\circ$ is that the associated FB arm ratings enable the PAC and SPM to achieve a quite wide PQ curve. More specifically, the PQ curve of the SPM approximates–and for some operating points surpasses–the ideal curve. The resulting ratings of the FB arms are summarized in Table II.

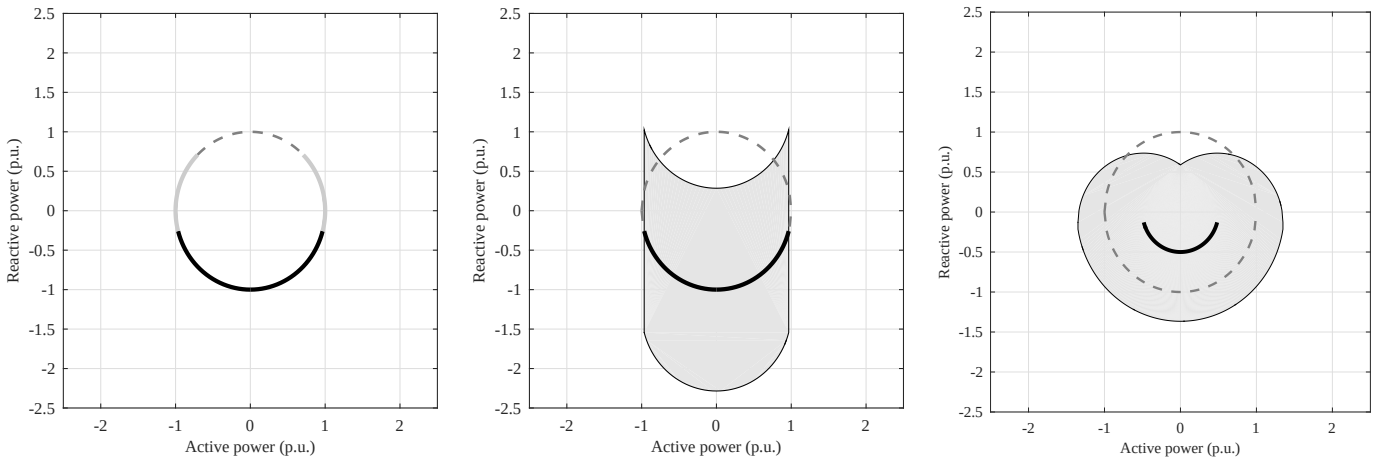

Fig. 12. PQ capability curve for SAC (left), PAC (middle) and SPM (right) topologies. All graphs show the achieved PQ curve extension (light gray line/area) over the LCC PQ curve for $\alpha = 15^\circ$ (black line) and the ideal PQ curve–representing the boundary of a PQ curve achieved by a VSC with apparent-power rating equal to S_{base}–(dashed gray line). The rating of all topologies estimated for achieving $\varphi = 45^\circ$ at $\alpha = 15^\circ$.

TABLE II
ESTIMATED REQUIRED RMS RATINGS OF FB ARMS FOR ACHIEVING $\varphi = 45^\circ$ WHILE $\alpha = 15^\circ$.

Topology	$\boldsymbol{V_{\mathrm{chl}}}$ **(p.u.)**	$\boldsymbol{I_{\mathrm{chl}}}$ **(p.u.)**	$\boldsymbol{S_{\mathrm{comb}}}$ **(p.u.)**	$\boldsymbol{S_{\mathrm{LCC}}}$ **(p.u.)**
SAC	0.9	1	1.8	1
SDC	0.9	1	3.6	0.48
PAC	1.05	1.22	2.6	1
SPM	0.57	1.7	4.6	0.5

The left graph of Fig. 12 depicts the PQ curve of the SAC and SDC topologies and shows that the active and reactive power of the SAC cannot be controlled independently. The operating point of the SAC and SDC topologies can be moved only over the gray and black curves, which leads to a change in both active and reactive power. The immediate implication is that on-load tap changing is needed for reducing the reactive-power consumption of the hybrid converter if the dc-link power must be low.

The PQ curve of the PAC is presented in the middle graph of Fig. 12, which shows that the operating point of the PAC topology can be anywhere in the gray area, while the operating points of the LCC can be only on the black curve. The dashed curve represents again the ideal PQ curve. Note that the maximum reactive power that can be generated is represented by the upper bound of the gray area in Fig. 12 (middle graph) and is related to the operating point of the LCC. This maximum capacitive reactive-power mode can be described by (33) if it is assumed that the FB arms are operating at their maximum capacitive reactive-power $Q_{\mathrm{fa,max}}$. This leads to

$$S_{\mathrm{hyb}}^2 = P_{\mathrm{LCC}}^2 + \left(Q_{\mathrm{fa,max}} - Q_{\mathrm{LCC}}\right)^2 . \tag{38}$$

Equation (38) represents a PQ curve similar with that of the LCC but offset by $Q_{\mathrm{fa,max}}$. Thus, as the firing angle α is approaching 90°, the capacitive reactive power of the PAC is reduced. Similarly, the maximum reactive power that can be consumed is represented by the lower bound of the gray area in Fig. 12 (middle graph).

Moreover, when the LCC is operating at minimum firing or extinction angles, which means close to the points $(P, Q) = (1, 0)$ or $(P, Q) = (-1, 0)$ respectively, the FB arms can be used to boost the apparent power of the converter beyond the ideal PQ curve by supplying full capacitive or inductive reactive power. This means that the reactive-power capability of the PAC topology is quite high when the LCC is operating at high active-power levels. Conversely, the reactive-power capability of the PAC topology is significantly reduced when the LCC is operating at low active-power levels or close to firing angle 90°. This is particularly important if on-load tap-changing is eliminated, which means that for low active-power transfer the LCC must operate at firing angles close to 90°. This is the reason why the control of active and reactive power is characterized as *partially independent* for the PAC topology.

The SPM topology offers also a *partially independent* control of active and reactive power but with slightly different characteristics than that of the PAC topology. The FB MMC in the SPM is connected in such a way so that it can handle both active and reactive power by modifying its dc-link voltage and by injecting current at the grid side of the LCC respectively. This means that the FB MMC is able to operate at its full PQ capability while the LCC operating point is anywhere along its PQ curve. The PQ capability of the SPM is illustrated in the right-hand graph of Fig. 12, which shows that the operating point of the SPM topology can be anywhere in the gray area. This graph is based on (37), which can be interpreted as a circular area, the center of which is defined by P_{LCC} and Q_{LCC}. Thus, the PQ curve of the SPM can be visualized as a circular area that can be moved by being centered anywhere along the LCC PQ curve. Based on this, the right-hand graph of Fig. 12 actually illustrates all the possible positions of the circular PQ area of the FB MMC with respect to the LCC PQ curve.

V. Overall Comparison of the Considered Hybrid Topologies

Finally the studied hybrid topologies can be compared based on the findings of the investigations presented so far, which are summarized in Table III. Note that the information included in Table III includes the required current capability of the FB arms (i.e., unidirectional, bidirectional, as shown in [25] for the half-bridge MMC), the combined-power rating for achieving $\varphi = 0-45°$, the apparent-power rating of the LCC and the PQ capability. In addition, Table III includes the same information for a pure FB MMC with the same active-power rating and the same ac-bus voltage as the SPM. Thus, the pure FB MMC can serve as a reference case.

Table III shows that the SAC is the hybrid topology with the minimum combined-power rating of the FB arms. This rating is doubled for the SDC. This is because two FB arms are needed per phase, instead of one in the case of the SAC. Nevertheless, the FB arms of the SDC are introduced at the dc side. This means that the FB arms of the SDC need to conduct the dc-link current and thus, can have unidirectional current capability. In this way some of the switches may be eliminated.

Moreover, the FB arms at the dc side may contribute to reducing the voltage stresses on the thyristors. As a result, the apparent-power rating of the LCC can be reduced according to the blocking voltage ratio k_{vb}, as defined in (11). On the other hand, the SAC does not allow such a reduction and additionally its voltage injection may lead to the increase of the voltage stresses on the thyristors, as for the capacitor-commutated converter (CCC). However, the SAC can be controlled so that the voltage stresses of the thyristors remain equal to that of a conventional LCC. In any case, since two FB arms are always in the conduction path for both the SAC and the SDC topologies, the reduced LCC rating should enable the SDC to operate with lower losses than the SAC.

Both the SAC and the SDC control the reactive power by means of voltage injection. However, voltage injection impacts the dc-link voltage and thus, the active power. Thus, the voltage injection allows both topologies to control the dc-link voltage but inhibits the independent control of active and reactive power. As a result, both of the these topologies offer a marginal enhancement of the PQ capability compared to a conventional LCC.

The PAC and SPM topologies exhibit significantly enhanced PQ capability by decoupling the control of active and reactive power. Note though that for both topologies, the required current and voltage ratings required for such a broad PQ curve are quite high, as depicted by Fig. 9 and Fig. 10. Aside from this, the combined-power rating of the FB arms is more favorable for the PAC topology. Thus, the PAC can be more preferrable in terms of rating and specifically when the desired φ is small, i.e., $\varphi < 25°$. In such case the combined-power rating of the FB arms for the PAC is half than for the SPM.

On the other hand, the apparent-power rating of the LCC can be reduced for the SPM topology, as the FB MMC is handling part of the active power. This reduction is dependent on the dc-link voltage ratio k_{v}. Even though this reduction may favor the SPM in terms of losses (especially for high power angles φ), quantitative studies are needed to draw confident conclusions.

Furthermore, the dc-link voltage of the SPM can be fully controlled by the FB MMC, provided that $k_{\mathrm{v}} = 0.5$. This allows the operation of the LCC at minimum reactive power and the regulation of the dc-link power via the FB MMC. This is not possible for the PAC, for which the dc-link voltage is controlled by the LCC.

Table III shows that the combined-power rating of the FB arms for a pure FB MMC is not much higher than that of the SPM for achieving $\varphi = 45°$. Even though the SPM may be favored in terms of losses, the pure FB MMC enables fully independent control of active and reactive power, eliminates undesired reactive-power consumption and has low filtering requirements. Thus, the pure FB MMC may be preferred in some cases. Nevertheless, the SPM can prove a competitive alternative to the pure FB MMC in case losses are of great importance. The same applies for the PAC for which the bulk of the active power is handled by the LCC. Both the PAC and SPM could prove even more beneficial as the required φ is reduced.

VI. Discussion

Another interesting feature of the SPM topology is that the oversizing of the FB MMC could be used for boosting the dc-link power, if reactive-power consumption of the LCC is not an issue. Note that this oversizing originates from the need to compensate the minimum reactive power of the LCC. This feature is referred to the regions of the PQ area that are beyond the ideal curve and is termed *active-power boosting mode*. Therefore, if there is no need to compensate the reactive power of the LCC, the full apparent-power rating of the FB MMC can be used for boosting the dc-link power transfer over 1 p.u. Furthermore, if the *active-power boosting* is not needed, a FB MMC with apparent-power rating equal to half of the dc-link power can be used. In such case, the PQ curve of the SPM could still be significantly extended than that of the LCC. Consequently, the SPM topology offers interesting possibilities for upgrades of exisiting LCC-based HVDC links, such as the replacement of one pole of a 12-pulse LCC-based HVDC station with a FB MMC.

Note that the FB arms of each hybrid topology can be used for additional functionalities, such as active filtering. More specifically, in the case of SAC, SDC, and SPM topologies, injection of suitable harmonic voltages may be employed for actively smoothing the dc-link voltage. Consequently, the dc-link harmonic currents can be effectively mitigated, leading to reduced electromagnetic interference and/or more relaxed design requirements for the dc-link inductor. In fact, the active filtering should address low-order harmonics that the inductor cannot eliminate effectively. Therefore, the FB arms can operate at low switching frequencies–for minimizing switching losses–and the inductor can be designed for filtering high-order harmonics.

Similarly, in the case of PAC and SPM topologies injection of harmonic currents may be utilized for active filtering of

TABLE III
HYBRID TOPOLOGY COMPARISON - ESTIMATED REQUIRED RMS RATINGS OF FB ARMS FOR ACHIEVING $\varphi = 0 - 45^\circ$ WHILE $\alpha = 15^\circ$.

Topology	FB Chainlink Current Capability	FB Chainlink Combined-Power Rating	LCC Apparent-Power Rating	PQ Capability	Control of DC-Link Voltage by FB Chainliks
SAC	Bidirectional	$0.5 - 1.8$	1	Similar to LCC	Possible
SDC	Unidirectional	$1 - 3.6$	Dependent on k_{vb}	Similar to LCC	Possible
PAC	Bidirectional	$0.5 - 2.6$	1	Partially Independent	Not Possible
SPM	Bidirectional	$3 - 4.6$	Dependent on k_{v}	Partially Independent	Possible
FB MMC	Bidirectional	5.4	Not Relevant	Independent	Possible

the current on the ac side. Again, the FB arms can be controlled to actively filter low-order harmonics, for which passive filters are rather bulky and costly, if sharp cutoff is required. Thus, the main benefits of active filtering on the ac side are smaller footprint and sharp cutoff of low-order harmonics that could propagate to the grid. The latter can be particularly advantageous if the hybrid converter is to be connected to weak grids. A notable flexibility offered by the PAC is that the active filtering and the reactive-power compensation functionalities can be decoupled and achieved by separate FB converters. In this way, each converter can be tailored to the associated functionality. In summary, even though the active filtering options were not analyzed in this paper, they open interesting questions for future studies.

VII. CONCLUSION

In this paper, four different hybrid topologies combining an LCC with FB arms were presented and compared in terms of combined-power rating and PQ capability. The comparative results show that the SAC requires the arms with the minimum rating. However, the arms of the SDC and SPM can be used to reduce the rating of LCC. Moreover, the PAC and the SPM are more flexible in terms of PQ capability, as the control of active and reactive power could be decoupled within the limits defined by the rating of the FB arms and FB MMC respectively. Due to this, on-load tap changing could be eliminated for the PAC and SPM topologies. The main difference between these two topologies is that the FB MMC in the SPM is capable of handling half of the active power of the dc-link and thus, the LCC power rating can be reduced to half. Finally, the overall comparison of the studied hybrid topologies showed that the PAC and the SPM can prove good alternatives to the pure FB MMC especially in cases where the required φ is low.

REFERENCES

[1] J. R. Toth, J. D. Schoeffler, and K. M. Chirgwin, "Artificial commutation of static converters," *Transactions of the American Institute of Electrical Engineers, Part I: Communication and Electronics*, vol. 82, no. 1, pp. 83–94, Mar. 1963.

[2] T. Gilsig and L. Freris, "Artificial Commutation of Converters Through Injection Technique," *IEEE Trans. Power App. Syst.*, vol. PAS-88, no. 7, pp. 1052–1061, Jul. 1969.

[3] J. Reeve, J. Baron, and G. Hanley, "A Technical Assessment of Artificial Commutation of HVDC Converters with Series Capacitors," *IEEE Trans. Power App. Syst.*, vol. PAS-87, no. 10, pp. 1830–1840, Oct. 1968.

[4] M. Meisingset, "A comparison of conventional and capacitor commutated converters based on steady-state and dynamic considerations," in *Seventh International Conference on AC and DC Transmission*, vol. 2001. IEE, 2001, pp. 49–54.

[5] A. Gole and M. Meisingset, "Capacitor commutated converters for long-cable HVDC transmission," *Power Engineering Journal*, vol. 16, no. 3, pp. 129–134, Jun. 2002.

[6] T. Tanaka, M. Nakazato, and S. Funabiki, "A new approach to the capacitor-commutated converter for HVDC-a combined commutation-capacitor of active and passive capacitors," in *2001 IEEE Power Engineering Society Winter Meeting. Conference Proceedings (Cat. No.01CH37194)*, vol. 2. IEEE, 2001, pp. 968–973.

[7] T. Isobe, D. Shiojima, K. Kato, Y. R. R. Hernandez, and R. Shimada, "Full-Bridge Reactive Power Compensator With Minimized-Equipped Capacitor and Its Application to Static Var Compensator," *IEEE Trans. Power Electron.*, vol. 31, no. 1, pp. 224–234, Jan. 2016.

[8] M. Jafar, M. Molinas, T. Isobe, and R. Shimada, "Transformer-Less Series Reactive/Harmonic Compensation of Line-Commutated HVDC for Offshore Wind Power Integration," *IEEE Trans. Power Del.*, vol. 29, no. 1, pp. 353–361, Feb. 2014.

[9] B. Franken and G. Andersson, "Analysis of HVDC converters connected to weak AC systems," *IEEE Trans. Power Syst.*, vol. 5, no. 1, pp. 235–242, 1990.

[10] O. Nayak, A. Gole, D. Chapman, and J. Davies, "Dynamic performance of static and synchronous compensators at an HVDC inverter bus in a very weak AC system," *IEEE Trans. Power Syst.*, vol. 9, no. 3, pp. 1350–1358, 1994.

[11] S. Bozhko, R. Blasko-Gimenez, R. Li, J. Clare, and G. Asher, "Control of Offshore DFIG-based Wind Farm Grid with Line-Commutated HVDC Connection," in *2006 12th International Power Electronics and Motion Control Conference*. IEEE, Aug. 2006, pp. 1563–1568.

[12] P. Fischer de Toledo, "Modelling and control of a line-commutated HVDC transmission system interacting with a VSC STATCOM," PhD Thesis, KTH Royal Institute of Technology, 2007.

[13] Honglin Zhou, Geng Yang, and Jun Wang, "Modeling, Analysis, and Control for the Rectifier of Hybrid HVdc Systems for DFIG-Based Wind Farms," *IEEE Trans. Energy Convers.*, vol. 26, no. 1, pp. 340–353, Mar. 2011.

[14] H. Jiang and A. Ekstrom, "Harmonic cancellation of a hybrid converter," *IEEE Trans. Power Del.*, vol. 13, no. 4, pp. 1291–1296, 1998.

[15] B. Qahraman and A. Gole, "A VSC based series hybrid converter for HVDC transmission," in *Canadian Conference on Electrical and Computer Engineering, 2005.* IEEE, 2005, pp. 458–461.

[16] B. Qahraman, A. Gole, and I. Fernando, "Hybrid HVDC converters and their impact on power system dynamic performance," in *2006 IEEE Power Engineering Society General Meeting*. IEEE, 2006, p. 6 pp.

[17] T. H. Nguyen, D.-C. Lee, and C.-K. Kim, "A Series-Connected Topology of a Diode Rectifier and a Voltage-Source Converter for an HVDC Transmission System," *IEEE Trans. Power Electron.*, vol. 29, no. 4, pp. 1579–1584, Apr. 2014.

[18] G. Andersson and M. Hyttinen, "Skagerrak: The Next Generation," in *CIGRE Symposium*, Lund, Sweden, 2015.

[19] A. Lesnicar and R. Marquardt, "An innovative modular multilevel converter topology suitable for a wide power range," in *2003 IEEE Bologna Power Tech Conference Proceedings*, vol. 3. IEEE, pp. 272–277.

[20] G. P. Adam, I. A. Abdelsalam, K. H. Ahmed, and B. W. Williams, "Hybrid Multilevel Converter With Cascaded H-bridge Cells for HVDC Applications: Operating Principle and Scalability," *IEEE Trans. Power Electron.*, vol. 30, no. 1, pp. 65–77, Jan. 2015.

[21] Jih-Sheng Lai and Fang Zheng Peng, "Multilevel converters-a new breed of power converters," *IEEE Trans. Ind. Appl.*, vol. 32, no. 3, pp. 509–517, 1996.

[22] J. Ainsworth, M. Davies, P. Fitz, K. Owen, and D. Trainer, "Static VAr compensator (STATCOM) based on single-phase chain circuit convert-

ers," *IEE Proceedings - Generation, Transmission and Distribution*, vol. 145, no. 4, p. 381, Jul. 1998.

[23] P. Bakas, L. Harnefors, S. Norrga, A. Nami, K. Ilves, F. Dijkhuizen, and H.-P. Nee, "Hybrid Topologies for Series and Shunt Compensation of the Line-Commutated Converter," in *8th International Power Electronics and Motion Control Conference - ECCE Asia, IPEMC 2016-ECCE Asia*. IEEE, 2016.

[24] N. G. Hingorani and L. Gyugyi, *Understanding FACTS : concepts and technology of flexible AC transmission systems*. IEEE Press, 2000.

[25] M. A. Perez, S. Bernet, J. Rodriguez, S. Kouro, and R. Lizana, "Circuit Topologies, Modeling, Control Schemes, and Applications of Modular Multilevel Converters," *IEEE Trans. Power Electron.*, vol. 30, no. 1, pp. 4–17, Jan. 2015.

[26] A. Nami, J. Liang, F. Dijkhuizen, and G. D. Demetriades, "Modular Multilevel Converters for HVDC Applications: Review on Converter Cells and Functionalities," *IEEE Trans. Power Electron.*, vol. 30, no. 1, pp. 18–36, Jan. 2015.

[27] J. Arrillaga, Y. H. Liu, and N. R. Watson, *Flexible Power Transmission: The HVDC Options*. John Wiley & Sons, 2007.

[28] K. Ilves, S. Norrga, and H.-P. Nee, "On energy variations in modular multilevel converters with full-bridge submodules for Ac-Dc and Ac-Ac applications," in *2013 15th European Conference on Power Electronics and Applications (EPE)*. IEEE, Sep. 2013, pp. 1–10.